Materials Research. 2025; 28:e20240506
DOI: https://doi.org/10.1590/1980-5373-MR-2024-0506

Comparative Study of the Addition of TiO_2 and TiO_2/OMMT Clay on the Properties of PBAT for Biodegradable Food Packaging Applications

Antônio de Assis Pereira Teles da Silva[a], *Regina Felipe do Ó*[a], *Luciana da Cunha Costa*[b], *Fernanda Abbate dos Santos*[a], *Gisele Cristina Valle Iulianelli*[a*]

[a]*Universidade Federal do Rio de Janeiro, Instituto de Macromoléculas Professora Eloisa Mano, Rio de Janeiro, RJ, Brasil.*
[b]*Universidade do Estado do Rio de Janeiro, Faculdade de Ciência Biológicas e Saúde, Departamento de Farmácia, Rio de Janeiro, RJ, Brasil.*

Received: November 06, 2024; Revised: May 04, 2025; Accepted: May 16, 2025

Microplastics from synthetic polymers significantly impact ecosystems and human health, making biodegradable polymers a promising alternative. To enhance their properties, nanofillers have been widely explored. In this study, TiO_2 nanoparticles, alone and combined with B8 OMMT clay, were incorporated into a PBAT matrix to improve its functionality for food packaging applications. Results revealed that nanofillers did not significantly alter PBAT's crystallinity (Xc ≈ 33%) or thermal stability (Tonset ≈ 375 °C), and the nanocomposites exhibited a predominantly intercalated morphology. Furthermore, low concentrations of nanofillers improved matrix uniformity. Contact angle measurements showed increased hydrophilicity in all formulations, with B8 OMMT systems exhibiting the highest hydrophilicity. The mechanical performance of the PBAT/B8/TiO_2 systems was more promising in terms of stiffness, with a 44% increase in Young's modulus for the PBAT/B8/TiO_2 0.5% system. However, all PBAT/B8/TiO_2 systems exhibited a more pronounced loss of ductility. Water activity (aW) analysis demonstrated that TiO_2 alone reduced aW values to 0.50–0.53, which could potentially enhance biosafety, while the addition of B8 OMMT increased aW to 0.69–0.76, potentially increasing susceptibility to microbial growth. Notably, systems with TiO_2 alone showed the greatest potential for food packaging applications due to their increased biosafety, thermal stability, and favorable set of properties.

Keywords: *PBAT, TiO_2, clay, nanocomposites, biodegradable food packaging.*

1. Introduction

In response to the environmental crisis caused by the accumulation of petroleum-based plastic and the associated generation of microplastics, which pose harmful consequences for ecosystems and human health, biodegradable polymers have emerged as a promising alternative[1]. Biodegradable polymers exhibit beneficial characteristics, including biocompatibility and low toxicity, making them particularly attractive for the packaging industry[2]. However, their practical applicability is limited by certain drawbacks, such as thermal instability, inadequate mechanical properties, poor gas barrier capabilities, and high production costs[3,4]. To overcome these challenges, the integration of nanotechnology with polymer science offers a potential solution, resulting in biodegradable polymer nanocomposites.

Among biodegradable polymers, poly(butylene adipate-co-terephthalate) (PBAT) exhibits promising properties. PBAT is a copolyester synthesized through the polycondensation of butanediol, adipic acid, and terephthalic acid, combining both aliphatic (from the butylene adipate group) and aromatic (from the butylene terephthalate group) segments in its linear chain, which confer flexibility and thermal stability[5,6]. Notably, PBAT offers excellent flexibility, high elongation at break and favorable processing properties[7]. Major companies such as BASF, Novamont, BIOTECH, and KINGFA have developed PBAT-based materials for a variety of packaging applications. The biodegradability of these polymers is primarily attributed to the ester bonds in their aliphatic groups, which are susceptible to hydrolysis; however, these same groups contribute to thermal instability. In contrast, the aromatic components enhance PBAT's mechanical properties. Its ability to degrade under both composting and soil conditions make PBAT a viable solution for combating plastic pollution. Consequently, PBAT is predominantly used in the production of environmentally friendly plastic films, supporting the development of sustainable alternatives to conventional plastics[7].

One current approach to addressing the mechanical and thermal limitations of biodegradable polymers involves incorporating metal oxide nanoparticles and organomodified clays into these polymer matrices. In this study, titanium dioxide nanoparticles (TiO_2 NPs) and an organomodified clay (Viscogel B8 Montmorillonite) were selected as nanofillers

*e-mail: gisele@ima.ufrj.br

for the PBAT matrix due to their attributes beneficial to packaging applications[8,9].

TiO_2 NPs are particularly valued for their chemical stability, water disinfection capability, and self-cleaning surface applications. Their antimicrobial efficacy of TiO_2 NPs has been demonstrated against gram-negative and gram-positive bacteria, as well as fungi, especially under UV light activation[10,11]. Additionally TiO_2 NPs exhibit remarkable oxidative properties, which are utilized in the photodegradation of organic compounds, water splitting to produce hydrogen, and UV light blocking[12,13]. These properties make TiO_2 NPs highly effective in extending the shelf life of packaged products, reducing food waste, and minimizing the need for chemical preservatives[14]. Various synthesis methods such as sol-gel, hydrothermal, and electrochemical routes, as well as chemical and physical vapor deposition techniques, enable the production of cost-effective and accessible TiO_2 nanostructures[13]. The incorporation of TiO_2 NPs into biodegradable polymer matrices for antimicrobial and UV-barrier functionality is well documented[11].

On the other hand, clays, particularly montmorillonite (MMT), are another widely used nanofiller in the preparation of nanocomposites. To enhance the interaction between polymers and these clays, chemical modifications, known as organophilization, are often applied, resulting in organophilized montmorillonite (OMMT). Previous studies have successfully incorporated OMMT nanostructures into biodegradable polymers, demonstrating enhancements in thermal stability, mechanical strength, and gas barrier properties in biodegradable polymers, allowing for thinner packaging materials and reduced raw material consumption[15,16]. These improvements not only address key challenges in biodegradable packaging but also align with sustainability principles, contributing to the development of more eco-friendly solutions.

In this study, TiO_2 nanoparticles were incorporated into the PBAT matrix in different proportions, both individually and in combination with Viscogel B8®, an OMMT organically modified with a quaternary alkyl ammonium compound (trimethyl-octadecyl ammonium salt)[11] to assess potential improvements in functional properties. The biodegradable polymer nanocomposites were characterized through various techniques, including X-ray diffraction (XRD), Fourier Transform Infrared Spectroscopy, Thermogravimetric Analysis (TGA), Differential Scanning Calorimetry (DSC), Contact angle measurement, Water activity (aW) assessment and Field emission gun scanning electron microscopy (FEG-SEM). The findings were analyzed and compared to identify the most promising formulation for advancing biodegradable materials within the packaging industry.

2. Experimental

2.1. Materials

Poly(butylene adipate-co-terephthalate) (PBAT) in pellet form, used as polymer matrix, was supplied by Ecoflex®. Titanium dioxide (TiO_2) nanoparticles were supplied by Sigma-Aldrich® with < 25 nm particle size and the organoclay Viscogel B8® (B8 OMMT) was supplied from Bentec (Livorno, Italy).

2.2. Preparation of the nanocomposites

Prior to melt processing, PBAT pellets were ground in a knife mill to optimize premixing with the nanofillers. Subsequently, the ground PBAT and B8 OMMT and TiO_2 nanoparticles were dried in an oven at 50 ºC for 3 hours. Different formulations of PBAT containing isolated TiO_2 NPs at concentrations of 0.1; 0.3 and 0.5 wt%; as well as formulations of PBAT containing B8 OMMT at a fixed ratio of 1 wt%, combined with TiO_2 NPs at 0.1, 0.3 and 0.5 wt% were subjected to mixing, using solid mixing equipment. The proportions of TiO_2 nanoparticles were selected based on previous studies and the literature[17-19]. Finally, the nanocomposites were prepared using a double-screw extruder equipped with seven heating zones (140 °C for the first zone, 150 °C for the second zone and 160 °C for the remaining five zones) at a screw speed of 120 rpm.

2.3. Characterization of the PBAT and its nanocomposites

The properties of the PBAT and its prepared nanocomposites were evaluated using X-ray Diffraction (XRD), Differential Scanning Calorimetry (DSC), Thermogravimetric Analysis (TGA), Fourier Transform Infrared Spectroscopy (FTIR), Field Emission Gun-Scanning Electron Microscopy (FEG-SEM), Water Activity (aW), Contact Angle measurement and Tensile Testing.

XRD was performed using Rigaku Ultima IV diffractometer with CuKα radiation generator (λ=0.154 nm, 40Kv, 120 mA) at room temperature, in the range of 2θ from 2° to 60° at a rate of 1°/min, and step of 0.05°. This technique was used to evaluate the crystalline profile and degree of crystallinity of the materials. Degree of crystallinity was determined using Origin®, by evaluating the ratio of the areas under the crystalline peak and the total area, according to the equation XC (%) = IC / (IC + IA) x 100, where Xc is the crystallinity degree; Ic is the sum of the areas under the crystalline peaks and IA is the area of the amorphous halo. The peaks were interpreted using Gaussian peak function.

DSC analyses were carried out using a TA Instruments Q1000 calorimeter (with a temperature accuracy of ±2 ºC) under a nitrogen flow rate of 50 mL/min. The samples were subjected to a first heating ramp from –30 to 200 ºC, followed by a cooling ramp from 200 to –30 ºC. After this heating/cooling cycle, the samples were subjected to a second heating ramp from –30 to 200 ºC. The heating and cooling ramps were all performed at a scanning rate of 10 °C/min. The crystallization temperature (Tc), the glass transition temperature (Tg), and the melting temperature (Tm) were determined from second cooling and heating curves.

TGA measurements were performed using a TA Instruments Q500 calorimeter (with a temperature accuracy of ±2 °C). The samples were placed in a platinum holder under continuous nitrogen flow rate of 60 mL min^{-1} and heated at the rate of 10 ºC/min from 20 to 700 ºC. From this analyses, two parameters were measured to determine the thermal stability of the prepared samples: the initial degradation temperature (Tonset), determined as the lowest temperature at which thermal degradation is observed, and the temperature associated with the maximum thermal degradation (Tmax), obtained from the peak of DTG graph

and interpreted as the temperature in which the rate of mass loss is maximized.

FTIR spectroscopy was performed using a PERKIN ELMER Frontier spectrometer (V. 10.4.2), operating in attenuated total reflectance (ATR) mode, covering the range of 4000-400 cm^{-1}, with a spectral resolution of 4 cm^{-1} and 60 scans.

The morphological analysis of the nanocomposites was performed using a Field Emission Gun Scanning Electron Microscope (FEG-SEM) of TESCAN, model MIRA, 4th generation - equipped with FEG Schottky, LMU, LowVac Mode that allows the variation of low vacuum from 1 to 700 Pa. The samples were subjected to cryogenic breakdown and their surfaces were covered with an ultrathin layer of gold (in Sputter Coater BAL-TEC SCD005) at 30 mA current for 150 seconds in order to provide conductivity, before analysis.

Water activity (aW) was measured in an AquaLab (4 TE), METER Group LatAm Ltda, equipped with a dew point system at 25 °C. The films were assessed in the sample holder as they were obtained, without any type of preparation.

Contact-angle measurements were performed in a goniometer with the optical contact angle (Θ) measuring and contour analysis systems of the OCA 15 EC (Dataphysics Instruments), using at least five drops per sample. The experiment was carried out at 20 ºC, with a drop of distilled water of 5 µL, deposited on a sample surface, in the form of a film.

Mechanical properties were evaluated by tensile testing, using an Instron universal testing machine (model 5569). Specimens were prepared by compression molding at 140 °C for 5 minutes under 6 tons of pressure, using a mold conforming to the ASTM D638 Type V standard, with a thickness of 1 mm. Prior to testing, all samples were conditioned for 48 hours at 25 °C and 50% relative humidity. Five specimens per formulation were tested under these conditions. A 1 kN load cell and a crosshead speed of 50 mm/min were used. The Young's modulus, maximum tensile strength, and elongation at break values were reported as the arithmetic mean of the five specimens.

3. Results and Discussion

3.1. X-ray Diffraction (XRD)

Figure 1 (A) and (B) depict the X-ray diffraction (XRD) patterns obtained for PBAT/TiO_2 nanocomposites and PBAT/B8/TiO_2 nanocomposites, including neat PBAT and nanofillers, respectively. For neat PBAT (Figure 1 (A) and (B)) characteristic peaks were observed at 2θ = 16.35°, 17.51°, 20.5°, 23.23° and 24.87° attributed to the (011), (010), (101), (100) and (111) crystalline planes, respectively, confirming its semicrystalline nature[17]. The TiO_2 nanoparticles exhibited characteristic peaks of the anatase phase at 2θ = 25° and 48°, corresponding to the (101) and (200) planes, respectively[17,20]. The PBAT/TiO_2 nanocomposites showed the same peaks found in neat PBAT, however no distinct peaks corresponding to TiO_2 nanoparticles were observed. This absence may be attributed to the overlap of the PBAT peak at 2θ = 24.87° (111) plane with the TiO_2 peak at 2θ = 25° (101) plane, potentially obscuring the TiO_2 signal. Another possibility is the limited sensitivity of the XRD equipment to detect small amounts of TiO_2 nanoparticles (0.1–0.3 wt%) within the formulations. Similar studies examining the interaction of oxide nanoparticles within PBAT matrices have reported that the characteristic peaks of the nanoparticles become discernible only at higher concentrations relative to the PBAT matrix[21-23].

In Figure 1 (B), the characteristic peaks of OMMT B8 are presented. The peak at 2θ = 3.55° (d001) is attributed to the incorporation of the organophilic group between the clay lamellae during the organophilization process[24], which allows for the calculation of the average distance between the clay lamellae using Bragg's equation: $n\lambda = 2d \sin(\theta)$[25]. The calculated (d001) spacing for OMMT B8 was approximately 2.52 nm. This peak was analyzed in the nanocomposites to assess the potential for an intercalated or exfoliated morphology. According to Figure 1 (C), which provides a more detailed view of the d001 peak for B8 and its nanocomposites, this peak shifted to a lower angle of approximately 2θ = 2.4º, corresponding to an interlamellar distance of 3.7 nm. This result indicates an increased spacing between the clay lamellae, which is attributed to the presence of polymer molecules in this space. Therefore, the predominant morphology was intercalated, suggesting good interaction between PBAT and OMMT B8 in forming nanocomposites.

The crystallinity of the samples was also measured and compared to neat PBAT (Figure 1 (A) and (B)). It was observed that the presence of nanoparticles did not significantly alter the degree of crystallinity of the PBAT matrix, which was Xc = 33%, with a slight increase observed in the PBAT/B8/TiO_2 0.1 wt% sample (Xc%=36). Maintaining crystallinity

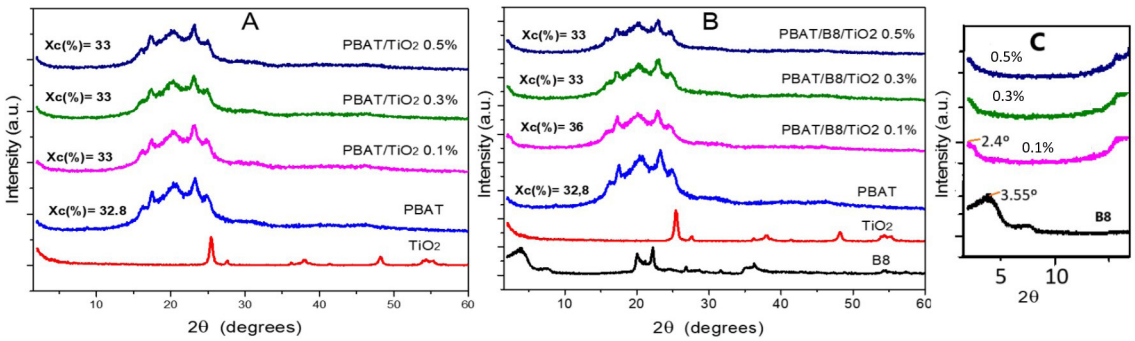

Figure 1. XRD patterns of PBAT/TiO_2 nanocomposites (A), PBAT/B8/TiO nanocomposites (B) and (C) Magnified view of image B.

is advantageous for packaging applications, since it is often linked to improved barrier properties in polymeric materials.

3.2. Thermal properties

The influence of TiO_2 nanoparticles, both individually and in combination with B8 OMMT, on the thermal properties of neat PBAT was investigated using DSC and TGA analyses, and the results are presented in Table 1.

Regarding DSC results (Table 1) and considering the equipment's margin of error (± 2 °C), there were no significant changes in the glass transition temperatures (Tg), crystallization temperature (Tc) and melting temperature (Tm). These findings suggest that, for the formulations tested, the nanoparticles did not affect the mobility of the PBAT matrix in either the amorphous or crystalline phases.

According to TGA results (Table 1 and Figures 2 and 3), the addition of nanoparticles did not significantly alter the Tonset or Tmax of the PBAT matrix, with exception of PBAT/B8/TiO_2 0.1 wt% sample, which showed a slight increase of approximately 6 ºC in Tonset and 7 ºC in Tmax.

This preservation of thermal stability, as evidenced by both, degradation temperature obtained from TGA and

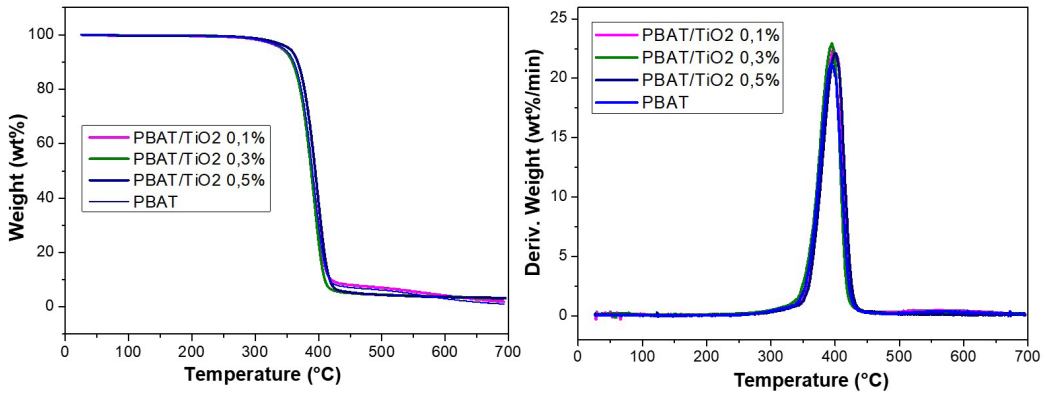

Figure 2. TG and DTG curves obtained for PBAT/TiO_2 nanocomposites.

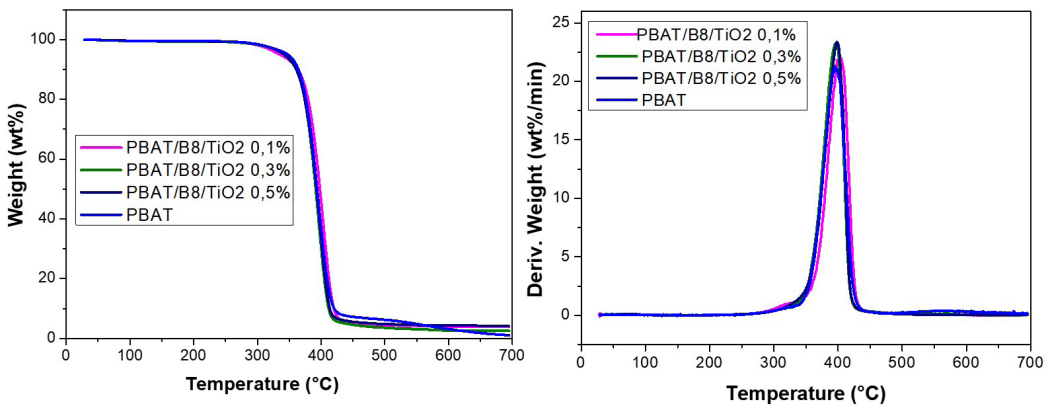

Figure 3. TG and DTG curves obtained for PBAT/B8/TiO_2 nanocomposites.

Table 1. Thermal properties of PBAT and its nanocomposites.

Samples	Tg (ºC)	Tc (ºC)	Tm (ºC)	Tonset (ºC)	Tmax (ºC)
PBAT	-32	98	122	370	395
PBAT/TiO_2 0.1	-32	95	123	372	397
PBAT/TiO_2 0.3	-32	96	121	370	397
PBAT/TiO_2 0.5	-32	97	122	372	399
PBAT/B8/TiO_2 0.1	-31	92	121	376	403
PBAT/B8/TiO_2 0.3	-32	93	122	370	397
PBAT/B8/TiO_2 0.5	-32	94	123	371	398

the thermal transition points from DSC, suggests that the incorporation of TiO_2 and B8 OMMT as nanofillers does not compromise the thermal behavior of PBAT. These results support its suitability for applications requiring stable thermal properties, such as in biodegradable packaging materials.

3.3. Fourier Transform Infrared Spectroscopy (FTIR)

The spectra of PBAT/TiO_2 and PBAT/B8/TiO_2 samples are shown in Figure 4 (A) and (B), respectively. Characteristic PBAT bands were identified across all nanocomposite samples. The bands at approximately 717 cm^{-1} and 808 cm^{-1} correspond to C–H aromatic rings and para-substitution of aromatic rings, respectively. Those around 935, 1018, 1102 and 1267 cm^{-1} are attributed to aromatic ring in plane and C–O interaction. The bands at 1456 cm^{-1} and 1507 cm^{-1} are associated with CH_2–CH_2 in-plane bending and C=C aromatic ring stretching, respectively. The band near 1711 cm^{-1} corresponds to C=O groups, while those around 2958 cm^{-1} and 1410 cm^{-1} are associated with CH_2 stretching and bending vibrations[26-29].

It can be observed that the spectra reveal minimal presence of bands related to the B8 and TiO_2 nanofillers. The spectra in Figure 4 (A) display a band around 3500 cm^{-1}, corresponding to O–H bond vibrations in the sample with the highest TiO_2 concentration (PBAT/TiO_2 0.5 wt%). Bands in the 3100–3600 cm^{-1} range are generally attributed to stretching in water molecules bound to TiO_2 nanoparticles[30]. The absence of distinct bands related to TiO_2 and B8 may be due to the low concentrations of these nanofillers in the prepared systems.

3.4. FEG-SEM

The Field Emission Gun Scanning Electron Microscopy (FEG-SEM) images are presented in Figure 5 A-G. Figure 5 (A1) and (A2) shows the surface of the neat PBAT sample at magnifications of 5Kx and 10Kx, revealing a homogeneous appearance, dense structure, and uniformly

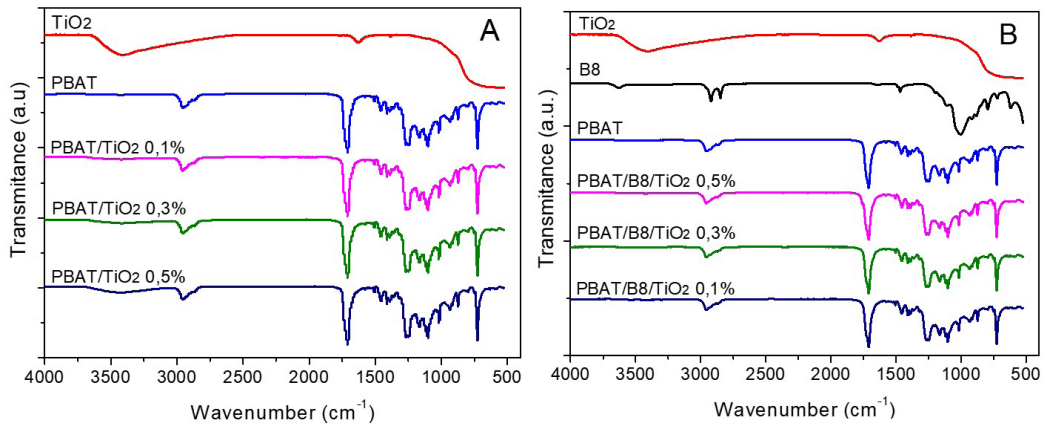

Figure 4. FTIR Spectra for the PBAT/TiO_2 nanocomposites (A) and PBAT/B8/TiO nanocomposites (B).

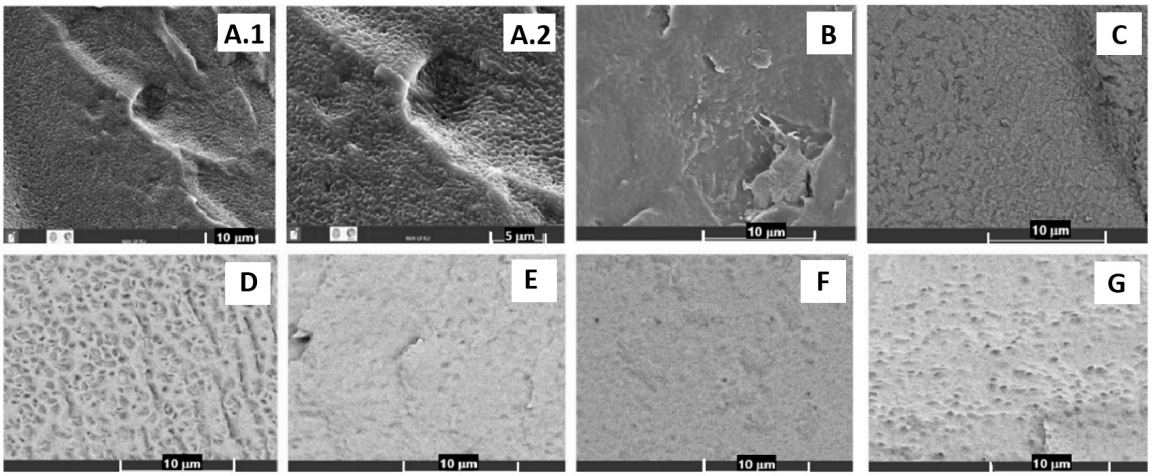

Figure 5. FEG-SEM images of neat PBAT (A) PBAT/TiO_2 systems containing 0.1 wt% (B), 0.3 wt% (C), and 0.5 wt% (D) of TiO_2 and PBAT/B8/TiO_2 systems containing 0.1 wt% (E), 0.3 wt% (F), and 0.5 wt% (G) of TiO_2.

distributed spherical formations. These formations may correspond to spherulites typical of the semicrystalline matrix or air microbubbles resulting from the material's processing[31-33].

Figures 5 (B), 5 (C) and 5 (D) display images of PBAT/TiO_2 nanocomposites containing 0.1 wt%, 0.3 wt%, and 0.5 wt% of TiO_2 nanoparticles, respectively. The addition of 0.1 wt% TiO_2 resulted in a more uniform matrix compared to neat PBAT. This result suggests that at this proportion, TiO_2 nanoparticles can fill voids or disordered regions within the matrix, reducing discontinuities that could contribute to roughness. This "filling" effect can smooth the surface and promote a more cohesive and uniform matrix structure. However, with increasing addition of TiO_2 (0.3 wt% and 0.5 wt%), the spherical formations became progressively larger (Figures 5 (C) and 5 (D)), indicating increased surface roughness and a coarser texture. This increased roughness may impact the mechanical performance of the films, by creating stress concentration points, potentially reducing elongation at break and flexibility. Additionally, excessive surface roughness could affect consumer perception, particularly in applications where a smooth texture is preferred for handling and visual appeal. In packaging applications, a rougher surface could also influence barrier properties by modifying the contact area with external agents such as moisture and gases.

For the PBAT/B8/TiO_2 systems, the sample with 0.3 wt% TiO_2 showed the most uniform matrix, while the 0.5 wt% TiO_2 sample exhibited a rougher matrix. However, this roughness was less pronounced compared to the system PBAT/TiO_2 0.5 wt%. These findings suggest that the inclusion of B8 OMMT (1 wt%) in the PBAT/TiO_2 0.5 wt% system helps to create a more uniform matrix.

The results found by FEG-SEM revealed that higher amounts of TiO_2 (0.5 wt%) apparently affected the organization of PBAT chains, preventing a more regular morphology. This impact on the polymer structure can create surface variations, contributing to a rougher texture.

3.5. Water activity (aW) analysis

The water activity (aW) analysis quantifies the available water in a product that can support the growth of microorganisms, as well as chemical and enzymatic reactions. In food packaging, this parameter is critical for predicting and controlling the growth of microorganisms, such as bacteria, fungi, and yeasts, which can compromise food quality and safety. Tipically, aW values between 0.0 and 0.6 are considered safe for inhibiting the growth of pathogens and spoilage microorganisms[34,35].

Table 2 presents the aW values for neat PBAT, PBAT/TiO_2, and PBAT/B8/TiO_2 nanocomposites. Neat PBAT showed an aW value of 0.57, indicating a safe profile. The addition of TiO_2 nanoparticles decreased this value to a range between 0.50 and 0.53, enhancing the safety of the PBAT matrix. In contrast, the addition of B8 OMMT increased the aW to a range of 0.69 to 0.76, making the PBAT/B8/TiO_2 nanocomposites less suitable for food packaging due to the higher aW values. This increase is attributed to the hygroscopic nature of clay, which absorbs and retains water molecules from the surrounding environment.

3.6. Contact angle measurement

PBAT and its nanocomposites were assessed for surface wettability using contact angle measurements, where water droplets were deposited on film surfaces. Representative images of the measurements are shown in Figure 6, and the average values from five replicates are summarized in Table 3. The results indicate that neat PBAT exhibited hydrophobic behavior ($90^o < \theta < 150^o$). Conversely, the incorporation of TiO_2 or TiO_2/B8 OMMT increased the wettability of the samples, rendering the nanocomposites hydrophilic ($0^o < \theta < 90^o$)[36-38]. It was observed that addition of B8 further increased hydrophilicity, aligning with the aW results. This was anticipated due to the inclusion of another hydrophilic component in the PBAT/TiO_2 system. Although both TiO_2 and B8 OMMT possess surface hydroxyl groups, the clay demonstrates greater hygroscopicity than TiO_2 due to its inherently more porous structure[39].

3.7. Mechanical testing

The results obtained from the tensile mechanical tests, presented in Figure 7 and Table 4, showed that the isolated addition of TiO_2 nanoparticles at concentrations of 0.1, 0.3, and 0.5 wt% did not significantly affect the Young's modulus of the PBAT matrix (67.5 MPa). This indicates that, at the evaluated concentrations, TiO_2 nanoparticles alone have a limited reinforcing effect on the stiffness of the PBAT matrix. In contrast, systems containing B8 OMMT showed a clear trend of increasing Young's modulus with higher TiO_2 content, with increments of approximately 15% (77.6 MPa) and 44% (97.0 MPa) observed for the formulations containing 0.3 wt% and 0.5 wt% TiO_2, respectively. The improved performance of these systems is associated with

Table 2. Water activity analysis of neat PBAT and its nanocomposites.

Samples	aw (25 °C)
Neat PBAT	0.57
PBAT/TiO_2 0.1%	0.51
PBAT/TiO_2 0.3%	0.50
PBAT/TiO_2 0.5%	0.53
PBAT/B8/TiO_2 0.1%	0.76
PBAT/B8/TiO_2 0.3%	0.69
PBAT/B8/TiO_2 0.5%	0.69

Table 3. Contact angle measurement of PBAT and its nanocomposites.

Samples	Contact Angle (°)	Standard Deviation
Neat PBAT	91.4	1.8
PBAT/TiO_2 0.1%	84.4	3.4
PBAT/TiO_2 0.3%	80.5	0.5
PBAT/TiO_2 0.5%	76.9	1.7
PBAT/B8/TiO_2 0.1%	77.7	3.1
PBAT/B8/TiO_2 0.3%	78.1	2.6
PBAT/B8/TiO_2 0.5%	74.3	2.7

Table 4. Tensile properties of PBAT and its nanocomposites.

Samples	Young's modulus (MPa)	Maximum tensile strength (MPa)	Elongation at break (%)
PBAT	67.5 ± 8.2	18.1 ± 1.8	566.9 ± 29.2
PBAT/TiO_2 0.1%	71.3 ± 6.7	10.2 ± 0.4	312.8 ± 12.6
PBAT/TiO_2 0.3%	69.8 ± 5.2	10.1 ± 0.9	298.2 ± 38.7
PBAT/TiO_2 0.5%	69.4 ± 6.7	9.4 ± 0.9	302.6 ± 22.4
PBAT/B8/TiO_2 0.1%	66.1 ± 10.9	6.9 ± 0.8	181.7 ± 31.7
PBAT/B8/TiO_2 0.3%	77.6 ± 5.6	8.6 ± 0.9	198.6 ± 26.9
PBAT/B8/TiO_2 0.5%	97.0 ± 2.1	11.4 ± 0.9	212.6 ± 53.4

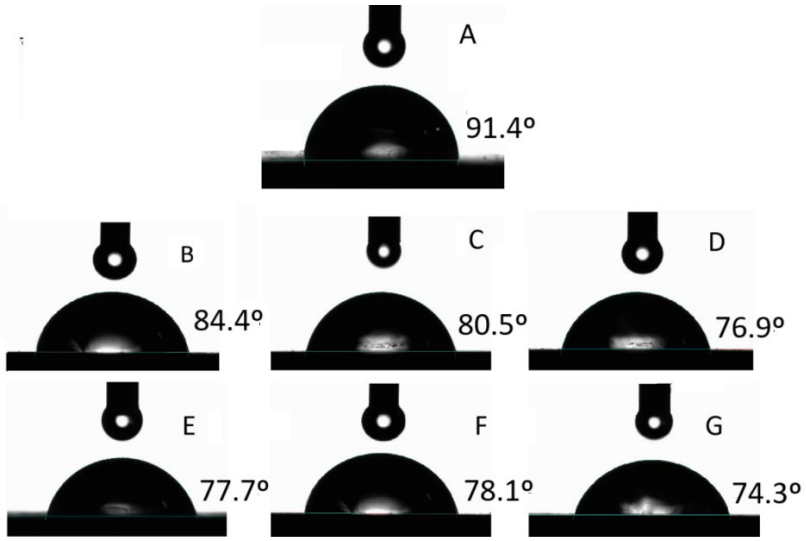

Figure 6. Sessile drop images obtained from contact angle measurements for neat PBAT (A) PBAT/TiO_2 systems containing 0.1 wt% (B), 0.3 wt% (C), and 0.5 wt% (D) of TiO_2 and PBAT/B8/TiO_2 systems containing 0.1 wt% (E), 0.3 wt% (F), and 0.5 wt% (G) of TiO_2.

the synergistic action between the organoclay and TiO_2, as evidenced by the more uniform morphology observed in FEG-SEM images, which suggested enhanced nanoparticle distribution and interfacial compatibility.

Regarding tensile strength, a significant reduction was observed for all formulations compared to neat PBAT (Figure 7 and Table 4). However, systems prepared with B8 exhibited a tendency toward increased tensile strength with rising TiO_2 content, mirroring the trend observed for Young's modulus. These findings further support the presence of a synergistic effect between the organoclay and TiO_2 nanoparticles, likely driven by improved nanoparticle dispersion and interfacial adhesion.

The results for elongation at break (ε) (Figure 7, red curve) showed a significant reduction in ductility for all nanocomposite systems when compared to neat PBAT (ε = 567%). This decrease is consistent with the incorporation of rigid nanofillers, which limit the mobility of polymer chains and consequently reduce the material's flexibility. In the PBAT/TiO_2 systems, ε values decreased to the range of 298%–332%, while in the systems containing both TiO_2 and B8 OMMT, values dropped further, ranging from 181% to 212%. Despite these reductions, the differences in elongation

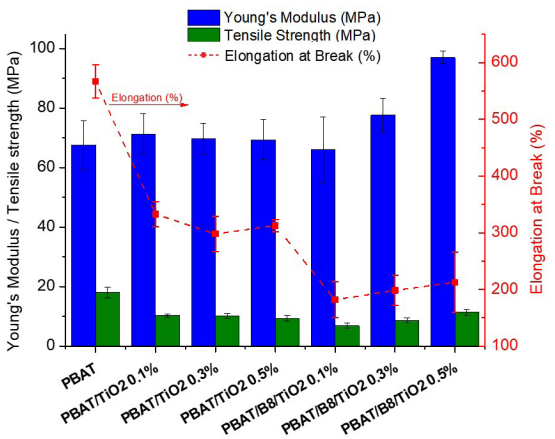

Figure 7. Young's modulus, maximum tensile strength and elongation at break of PBAT and its nanocomposites.

values among the different concentrations within each group were not statistically significant, as they were within the range of the standard deviation. These findings suggest

that although the presence of B8 OMMT clay contributes to improved dispersion of TiO_2 and better interfacial interactions, factors that enhance strength and stiffness, it also intensifies the restriction of chain mobility, thereby exacerbating the loss of ductility in the resulting nanocomposites.

4. Conclusion

This study investigated the effects of TiO_2 nanoparticles, both alone and in combination with OMMT B8 clay, on the properties of PBAT-based nanocomposites for packaging applications. XRD analysis revealed a predominantly intercalated morphology in PBAT nanocomposites, indicating good interaction between the nanofillers and polymer. Thermal analyses (DSC and TGA) showed that the addition of nanofillers did not significantly alter PBAT's thermal stability, which is favorable for packaging stability. Surface characterization by FEG-SEM revealed that low TiO_2 concentrations reduced PBAT's surface roughness, while higher concentrations increased it, potentially impacting the material's texture. Water activity (aW) measurements demonstrated that TiO_2 alone enhanced biosafety by reducing aW to levels that inhibit microbial growth, whereas the addition of OMMT B8 increased aW, compromising microbial resistance. Furthermore, contact angle measurements confirmed that both TiO_2 and OMMT B8 increased hydrophilicity, with PBAT/OMMT B8 systems displaying the highest levels. Mechanical testing showed that the addition of B8 OMMT clay combined with TiO_2 significantly increased Young's modulus for the PBAT/B8/TiO_2 0.5% formulation, representing a 44% improvement in stiffness compared to neat PBAT. However, this reinforcement was accompanied by a substantial reduction in ductility of these nanocomposite systems, which may compromise performance for food packaging applications.

Based on these findings, PBAT/TiO_2 nanocomposites, particularly those without clay, demonstrate a favorable balance between enhanced biosafety and overall properties, making them potential candidates for biodegradable packaging applications requiring microbial resistance. However, the observed increase in surface roughness at higher TiO_2 concentrations and with OMMT B8 addition suggests the need for further studies. Future research should also explore long-term biodegradation behavior and optimize nanofiller concentrations to maximize functional benefits while minimizing undesirable effects.

5. Acknowledgments

The authors would like to thank the Programa Institucional de Bolsas de Iniciação Científica of the Universidade Federal do Rio de Janeiro (PIBIC-UFRJ) for its financial support.

6. References

1. Mohanty AK, Misra M, Hinrichsen G. Biofibres, biodegradable polymers and biocomposites: an overview. Macromol Mater Eng. 2000;276-277(1):1-24.
2. Costa LV, Iulianelli GCV, Silva PSRC, Santos FA. Obtaining and characterization of biodegradable composites reinforced with microcrystalline cellulose fillers. Mater Sci Appl. 2021;12(12):561-77.
3. Harada J, Amorim CA, Braga PL, Machado LDB, Oliveira RR, Cabral A Neto, et al. Characterization of biodegradable mulch black films incorporated with organic fertilizers and rice husk ash. In: Proceedings of the 146th TMS Annual Meeting and Exhibition; 2017 February 26-March 2; San Diego, California. Proceedings. London: Springer; 2017.
4. Shaikh S, Yaqoob M, Aggarwal P. An overview of biodegradable packaging in food industry. Curr Res Food Sci. 2021;4:503-20.
5. Al-Itry R, Lamnawar K, Maazouz A. Rheological, morphological, and interfacial properties of compatibilized PLA/PBAT blends. Rheol Acta. 2014;53:501-17.
6. Jiao J, Zeng X, Huang X. An overview on synthesis, properties and applications of poly(butylene-adipate-co-terephthalate)–PBAT. Adv Ind Eng Polym Res. 2020;3(1):19-26.
7. Karimi A, Rahmatabadi D, Baghani M. Direct pellet three-dimensional printing of Polybutylene Adipate-co-Terephthalate for a greener future. Polymers. 2024;16(2):267.
8. Van Nguyen S, Lee BK. PVA/CNC/TiO2 nanocomposite for food-packaging: improved mechanical, UV/water vapor barrier, and antimicrobial properties. Carbohydr Polym. 2022;298:1-10.
9. Dornelas CB, Resende DK, Rocha HVA, Gomes AS, Tavares MIB, Coutinho SSS, et al. Avaliação de derivados poliméricos intercalados em montmorilonita organofílica na preparação de novos materiais de uso farmacêutico. Polímeros. 2008;18(3):222-9.
10. Ahmed RM, Hasan I. A review on properties and applications of TiO_2 and associated nanocomposite materials. Mater Today Proc. 2023;81(2):1073-8.
11. Ali I, Suhail M, Alothman ZA, Alwarthan A. Recent advances in syntheses, properties and applications of TiO_2 nanostructures. RSC Advances. 2018;8(53):30125-47.
12. Mesgari M, Aalami AH, Sahebkar A. Antimicrobial activities of chitosan/titanium dioxide composites as a biological nanolayer for food preservation: a review. Int J Biol Macromol. 2021;176:530-9.
13. Berardinelli A, Parisi F. TiO_2 in the food industry and cosmetics. In: Parrino F, Palmisano L, editors. Titanium dioxide (TiO_2) and its applications. Amsterdam: Elsevier; 2021. p. 353-71.
14. Phothisarattana D, Wongphan P, Promhuad K, Promsorn J, Harnkarnsujarit N. Biodegradable poly (Butylene Adipate-Co-Terephthalate) and Thermoplastic Starch-Blended TiO2 nanocomposite blown films as functional active packaging of fresh fruit. Polymers. 2021;13(23):4192.
15. Shar AS, Zhang C, Song X, Weng Y, Du Q. Design of novel PLA/OMMT films with improved gas barrier and mechanical properties by intercalating OMMT interlayer with high gas barrier polymers. Polymers. 2021;13(22):3962.
16. Król-Morkisz K, Pielichowska K. Thermal decomposition of polymer nanocomposites with functionalized nanoparticles. In: Pielichowski K, Majka TM, editors. Polymer composites with functionalized nanoparticles. Amsterdam: Elsevier; 2019. p. 405-35.
17. Ferreira CSG, Silva e Souza P, Rodrigues JGP, Silva EO, Tavares MIB, Iulianelli GCV. Development of biodegradable PBAT matrix nanocomposites incorporated with nanoparticulate TiO_2 and assessment of their properties for application in food packaging. Obs Econ Latinoam. 2024;22(1):3136-58.
18. Iulianelli GCV, David GS, Santos TN, Sebastião PJO, Tavares MIB. Influence of TiO2 nanoparticle on the thermal, morphological and molecular characteristics of PHB matrix. Polym Test. 2018;65:156-62.
19. Eshaghi R, Mohsenzadeh M, Ayala-Zavala JF. Bio-nanocomposite active packaging films based on carboxymethyl cellulose, myrrh gum, TiO2 nanoparticles and dill essential oil for preserving fresh-fish (Cyprinus carpio) meat quality. Int J Biol Macromol. 2024;263(Part 2):12991.

20. Thirugnanasambandan T, Alagar M. Titanium dioxide (TiO2) nanoparticles XRD analyses: an insight. ArXiv: Chemical Physics. 2013:1307.
21. Pascariu P, Cojocaru C, Samoila P, Airinei A, Olaru N, Rusu D, et al. Photocatalytic and antimicrobial activity of electrospun ZnO nanostructures. J Alloys Compd. 2020;834:1-11.
22. Pulikkalparambil H, Phothisarattana D, Promhuad K, Harnkarnsujarit N. Effect of silicon dioxide nanoparticle on microstructure, mechanical and barrier properties of biodegradable PBAT/PBS food packaging. Food Biosci. 2023;55:1-10.
23. Thiyagu TT, Gokilakrishnan G, Uvaraja VC, Maridurai T, Prakash VRA. Effect of SiO_2/TiO_2 and ZnO nanoparticle on cardanol oil compatibilized PLA/PBAT biocomposite packaging film. Silicon. 2022;14(7):3795-808.
24. Brito L, Tavares MIB. Evaluation of the influence of nanoparticles' shapes on the formation of Poly(lactic acid) nanocomposites obtained employing the solution method. J Nanosci Nanotechnol. 2012;12(6):4508-13.
25. Galeski A. Strength and toughness of crystalline polymer systems. Prog Polym Sci. 2003;28(12):1643-99.
26. Rocha LVM, Silva PSRC, Silva EMB, Aguiar VO, Tavares MIB. Biodegradable packing food films based on PBAT containing ZnO and MoO3. J Appl Polym Sci. 2024;141(17):e55294.
27. Zehetmeyer G, Meira SMM, Scheibel JM, Silva CB, Rodembusch FS, Brandelli A, et al. Biodegradable and antimicrobial films based on poly(butylene adipate-co-terephthalate) electrospun fibers. Polym Bull. 2016;8:3243-68.
28. Al-Itry R, Lamnawar K, Maazouz A. Improvement of thermal stability, rheological and mechanical properties of PLA, PBAT and their blends by reactive extrusion with functionalized epoxy. Polym Degrad Stabil. 2012;97(10):1898-914.
29. Almayah A. Use of gamma radiation techniques in peaceful applications. London: IntechOpen; 2019.
30. Buzarovska A. PLA nanocomposites with functionalized TiO_2 nanoparticles. Polym Plast Technol Eng. 2013;52(3):280-6.
31. Ferreira CSG, Souza P, Toma H, Silva E, Tavares MI, Iulianelli G. Influence of ZnO nanoparticles on the properties of biodegradable PBAT matrix for food packaging application. Concilium. 2023;23(18):226-40.
32. Spoială A, Ilie CI, Trușcă RD, Oprea OC, Surdu VA, Vasile BȘ, et al. Zinc oxide nanoparticles forwater purification. Materials. 2021;14(16):4747.
33. Wang R, Xie C, Zeng L, Xu H. Thermal decomposition behavior and kinetics of nanocomposites at low-modified ZnO content. RSC Advances. 2019;9(2):790-800.
34. Almasi H, Oskouie MJ, Saleh A. A review on techniques utilized for design of controlled release food active packaging. Crit Rev Food Sci Nutr. 2021;61(15):2601-21.
35. Tapia MS, Alzamora SM, Chirife J. Effects of water activity (aw) on microbial stability as a hurdle in food preservation. In: Barbosa-Cánovas GV, Fontana AJ Jr, Schmidt SJ, Labuza TP, editors. Water activity in foods: fundamentals and applications. 2nd ed. Hoboken: John Wiley & Sons, Inc.; 2020. p. 323-55.
36. Glier A, Trindade RS. O emprego de polmeros em revesitmenos hidrofbicos, super-hidrofbicos e autolimpantes: uma reviso da literatura. Disciplinarum Scientia. 2020;21(2):59-74.
37. Ferreira CSG, Silva e Souza PS, Lacerda DS, Silva EO, Tavares MIB, Iulianelli GCV. Estudo da incorporação do grafeno na matriz de PBAT para produção de filmes nanocompósitos biodegradáveis para embalagens alimentícias. Obs Econ Latinoam. 2024;22(1):3422-45.
38. Marmur A, Della Volpe C, Siboni S, Amirfazli A, Drelich JW. Contact angles and wettability: towards common and accuratet erminology. Surf Innov. 2017;5(1):3-8.
39. Yin Y, Cui Z, Zhang X, Song J, Zhang X, Chen Y, et al. Effects of clay content on non-linear seepage behaviors in the sand–clay porous media based on low-field nuclear magnetic resonance. Water. 2024;16(6):883.